Supporting Information

On-demand controlled bidirectional DNAzyme path for ultra-sensitive heavy metal ion detection

Jing Xu,[a] Yujin Li,[a,b] Futing Wang,[b] Xinqi Luo,[a] Wei Zhang,[f] Yifan Lyu,[b] Hongfen Yang,[e] Ren Cai,[b*] Weihong Tan[b,c,d]

[a] College of Chemistry and Chemical Engineering, Xinyang Normal University, Dabie Mountain Laboratory, Xinyang 464000, China.

[b] Molecular Science and Biomedicine Laboratory, State Key Laboratory for Chemo/Bio-Sensing and Chemometrics, College of Material Science and Engineering, College of Chemistry and Chemical Engineering, College of Biology, Hunan University, Changsha, 410082, China.

[c] The Cancer Hospital of the University of Chinese Academy of Sciences (Zhejiang Cancer Hospital), Hangzhou Institute of Medicine, Chinese Academy of Sciences, Hangzhou, Zhejiang 310022, China.

[d] Institute of Molecular Medicine, Renji Hospital, Shanghai Jiao Tong University School of Medicine, and College of Chemistry and Chemical Engineering, Shanghai Jiao Tong University, Shanghai 200240, China.

[e] Hunan Key Laboratory of Typical Environmental Pollution and Health Hazards, School of Public Health, Hengyang Medical School, University of South China, Hengyang, Hunan 421001, China.

[f] College of Life Science, Xinyang Normal University, Dabie Mountain Laboratory, Xinyang 464000, China.

* To whom correspondence should be addressed. Email: cairen@hnu.edu.cn.

Contents

Chemicals

The DNA sequences of oligonucleotides (**Table S1**) were purchased from Shanghai Shenggong Biotechnology Co., Ltd. Bovine Serum Albumin (BSA, A8010-10g, ≥ 96%), 1-ethyl-3-(3'-dimethylaminopropyl) carbodiimide (EDC, ≥ 98%), N-hydroxysuccinimide (NHS, ≥ 98%), glucose oxidase (GOD, BR, 100-250 U/mg), hexammineruthenium (III) chloride ($[Ru(NH_3)_6]^{3+}$, ≥ 98%), diethylprocarbonate (DEPC, ≥ 99%), chloroauric acid tetrahydrate ($HAuCl_4 \cdot 3H_2O$, ≥ 99%), 4-(N-maleimidomethyl) cyclohexane-1-carboxylic acid 3-sulfo-N-hydroxysuccinimide ester sodium salt (sulfo-SMCC, ≥ 99%), phosphate buffered saline (PBS), sodium citrate (≥ 99%), monosodium dihydrogen phosphate (NaH_2PO_4, ≥ 99%), ethanol (C_2H_6OH, ≥ 99%), and disodium hydrogen phosphate (Na_2HPO_4, ≥ 99%) were obtained from Sinopharm Chemical Reagent Co. Ltd (Shanghai, China). The carbon paper (CP) (WOS1009) was purchased from Sigma-Aldrich. Potassium ferrocyanide trihydrate ($K_4[Fe(CN)_6]$, ≥ 99.95%), potassium ferricyanide ($K_3[Fe(CN)_6]$, ≥ 99.5%), potassium chloride (KCl, ≥ 99. 5%), $CuSO_4 \cdot 5H_2O$ (≥ 99%), NaOH (≥ 97%), sodium chloride (AR, 99.5%), ascorbic acid (≥ 99%), $Na_2S \cdot 9H_2O$ (AR, 99%), $Na_2S_2O_3 \cdot 5H_2O$ (AR, 99%), dopamine hydrochloride (≥ 98%), L-cysteine (≥ 99%), ammonium molybdate tetrahydrate (AR, 99%), tris buffer solution (0.01 M) were purchased from McLean Biochemical Reagent Co., Ltd.

The $[Fe(CN)_6]^{3-/4-}$ solution for the electrochemical tests consisted of 10 mM $K_4Fe(CN)_6$, 10 mM $K_3Fe(CN)_6$, and 0.1 M KCl. The buffer solutions for the experiment were as follows: phosphate buffered solutions (PBS) consisted of 0.1 M NaCl, 0.1 M Na_2HPO_4, and 0.1 M NaH_2PO_4 (pH 7.4). The TE buffer consisted of 10 mM Tris-HCl, 1 mM EDTA, and 12.5 mM $MgCl_2$ (pH 8). The above buffers were used with 0.1 M of HCl or 0.1 M of NaOH solution to regulate the pH.

Experimental Section

Synthesis of MoS_2@CuS heterostructures

First, 0.4981 g (1.99 mmol) $CuSO_4 \cdot 5H_2O$ and 0.5161 g (2.00 mmol) sodium citrate were dissolved in 320 mL deionized water and stirred for 30 min. Then, 80 mL NaOH (1.25 M) was added to the above solution and stirred for 30 min. Next, 200 mL ascorbic acid solution (3.00 M) was slowly added to the above solution and aged for 1 h at room temperature. The final product was washed and collected centrifugally with ethanol and deionized water, and dried for 12 h at 80 ℃.

Cu_2O nanocubes (0.5 g) were dispersed in 300 mL deionized water. Next, 100mL Na_2S aqueous solution (6.25 mM) was added to the above solution and stirred for 30 min at room temperature. The as-obtained product was washed several times with water and ethanol, and dried for 12 h at 80 ℃.

The as-prepared Cu_2O@CuS nanocubes (0.5 g) were dispersed in 100 mL ethanol/H_2O (1:1) solvent. Then, 80 mL $Na_2S_2O_3$ solution (1 M) was added to the above solution and stirred for 30 min at room temperature. The precipitate was collected by centrifugation, washed several times, and vacuum dried for 12 h at 80 ℃ to obtain hollow CuS nanocubes.

Hollow CuS nanocubes (0.06 g), 0.06 g ammonium molybdate tetrahydrate and 6 g L-cysteine were dissolved in 75 mL deionized water with stirring for 3 h at room temperature. The solution was transferred to an autoclave, and reacted for 24 h at 220 ℃. After cooling, the product was alternately cleaned with ethanol and deionized water several times, and vacuum dried for 12 h to obtain the final product of MoS_2@CuS heterostructures.

Synthesis of AuNPs

First, 20 μL $HAuCl_4 \cdot 3H_2O$ solution (1%) was dropped into 50 mL deionized water, and heated to 110 ℃. Then, 500 μL $Na_3C_6H_5O_7 \cdot 2H_2O$ (1%) was quickly added to the above solution. The color of the solution gradually turned red, and heating was continued for another 10 min. Then, the final solution was stirred and cooled to room temperature. The as-prepared AuNPs were stored in the dark at 4 ℃.

Synthesis of AuNPs/MoS_2@CuS heterostructures

One mg MoS_2@CuS heterostructures was dispersed in 8 mL deionized water. The solution was mixed with 1 mL ethanol and 1 mL AuNPs solution under oscillation at room temperature to obtain AuNPs/MoS_2@CuS heterostructures.

Synthesis of DNAzyme

DNAzyme, a double-strand DNA (S1-S2), was synthesized by the hybridization of DNA S1 (500 μL, 2 μM) and DNA S2 with enzyme sites (500 μL, 2 μM) for 5 min at 95 ℃.

Synthesis of HCR

Hairpin H1 (25 μL, 2 μM) and hairpin H2 (25 μL, 2 μM) were mixed and incubated for 60 min at 37 ℃ to obtain the HCR product (H1, H2).

Preparation of the bioanode

First, carbon paper (CP, 1 cm × 1 cm) was immersed in HNO_3 (69 %) for 90 min and washed with DI-water several times. Then, 50 μL AuNPs/MoS_2@CuS solution (0.1 mg/mL) was dropped onto the CP surface and dried at 37 ℃ for 2 h to obtain AuNPs/MoS_2@CuS/CP. Next, 30 μL EDC/NHS (1 mg/mL) was added to the surface of AuNPs/MoS_2@CuS/CP and incubated for 30 min to activate AuNPs by conjugating -COOH groups from EDC/NHS. Then, 50 μL DNAzyme (i.e., S1-S2, 1 μM) was immobilized on the surface of the as-activated AuNPs/MoS_2@CuS/CP by Au-S bonding at 4 °C for 12 h to obtain DNAzyme/AuNPs/MoS_2@CuS/CP. Bovine albumin (BSA, 1 mg/mL, 50 μL) was used to avoid non-specific adsorption on DNAzyme/AuNPs/MoS_2@CuS/CP. Next, 50 μL Pb^{2+} solution (1 pM) was dropped onto the surface of DNAzyme/AuNPs/MoS_2@CuS/CP and incubated at 37 °C for 80 min to obtain Pb^{2+}/DNAzyme/AuNPs/MoS_2@CuS/CP. Here, Pb^{2+} cleaves the active sites of S2. Finally, the resulting Pb^{2+}/DNAzyme/AuNPs/MoS_2@CuS/CP is incubated with 50 μL S3-GOD (1 μM, see Supporting Information) at 37 °C for 80 min to obtain the bioanode, S3-GOD/Pb^{2+}/DNAzyme/AuNPs/MoS_2@CuS/CP by hybridization of S3 and S2 of DNAzyme at 37 ℃.

Preparation of the biocathode

Fifty μL S4 (1 μM) was added to the surface of as-activated AuNPs/MoS_2@CuS/CP at 4 ℃ for 12 h to obtain S4/AuNPs/MoS_2@CuS/CP, with 50 μL bovine albumin (BSA, 1 mg/mL) to avoid non-specific adsorption. Next, 50 μL S5 (1 μM) and 50 μL Hg^{2+} solution (1 pM) was dropped on the surface of S4/AuNPs/MoS_2@CuS/CP and incubated at 37 ℃ for 70 min to obtain S5-Hg^{2+}/S4/AuNPs/MoS_2@CuS/CP by forming a T-Hg^{2+}-T structure between S4 and S5. Finally, the HCR product (H1, H2 mixture, 50 μL, 1 μM) was fixed on S5-Hg^{2+}/S4/AuNPs/MoS_2@CuS/CP to obtain H1, H2/S5-Hg^{2+}/S4/AuNPs/MoS_2@CuS/CP at 37 °C after 90 min incubation, thus, triggering the HCR reaction to from abundant double-stranded DNA.

Preparation of the self-powered biosensor

The self-powered biosensor was fabricated with the bioanode, i.e., S3-GOD/Pb^{2+}/DNAzyme/AuNPs/MoS_2@CuS/CP, and the biocathode, i.e., H1, H2/S5-Hg^{2+}/S4/AuNPs/MoS_2@CuS/CP. The Pb^{2+} or Hg^{2+} is identified by the DNAzymes when either Pb^{2+} or Hg^{2+} is present. In the self-powered biosensor, a catalytic

oxidation reaction of glucose ($\mathrm{Glucose + O_2 + GOD \rightarrow Gluconic\ acid + H_2O_2}$) occurs at the bioanode simultaneously with the reduction reaction: $[Ru(NH_3)_6]^{3+} + e^- \rightarrow [Ru(NH_3)_6]^{2+}$ at the biocathode. Pb^{2+} and Hg^{2+} are monitored at the bioanode and biocathode by observing electrochemical currents, respectively. Finally, the self-powered biosensor quasi-simultaneously detects Pb^{2+} and Hg^{2+} by testing the open-circuit voltage (E^{ocv}).

Characterization

Transmission electron microscopy (TEM) and scanning electron microscopy (SEM) images of MoS_2@CuS heterostructures and AuNPs/MoS_2@CuS heterostructures were obtained on a JEOL TEM (JEM-2100Plus, Japan) and a JEOL SEM (JSM-6360LA, Japan), respectively. The UV–vis absorption spectra were acquired using UV-2450 spectrophotometer (Shimadzu Co., Ltd., Japan). Fourier transform infrared spectroscopy (FTIR) characterizations were carried out on a Nicolet In10 (Thermo Fisher, USA). The X-ray photoelectron spectroscopy (XPS) spectra of AuNPs/MoS_2@CuS heterostructures were studied with an AXIS SUPRA+ (Shimadzu Co., Ltd., Japan). Electrochemical impedance spectroscopy (EIS), cyclic voltammetry (CV), differential pulse voltammetry (DPV), linear sweep voltammetry (LSV), and open circuit voltage (E^{ocv}) were studied with a CHI 660E electrochemical workstation (Chenhua Instrument Shanghai Co., Ltd., China). E^{ocv} was measured in a biocathode and bioanode two-electrode system with 0.1 M phosphate solution (pH=7.4, containing 5 mM glucose and 500 μM $[Ru(NH_3)_6]^{3+}$).

Limit of detection calculation

The limit of detection (LOD) is calculated based on LOD = (Mean + $3S_D$)/k. Here, the mean is the detection average value of ten parallel measurements, S_D is the standard deviation of ten parallel controlled measurements, and k is the signal-to-noise ratio of 3.

For Pb^{2+} detection in CV test, the mean = 1.51 mA, S_D = 0.113, k_1 = 3, and the smallest detectable current (I) was calculated as: $I_{LOD} = b + kS_D$ = 1.855 mA. According to the linear regression equation: I = 0.01 lg C_{Pb2+} + 0.2, the LOD_1 was calculated to be 3.1 fM.

For Hg^{2+} detection in DPV test, the mean = 0.92 mA, S_D = 0.078, k_1 = 3, and the

smallest detectable current (I) absorption was calculated as: I_{LOD} = mean + kS_D = 1.15. According to the linear regression equation: I= 0.1 lg C_{Hg2+} + 2.4, the LOD_2 was calculated to be 0.32 pM.

In the bidirectional detection of Pb^{2+} and Hg^{2+} process, for Pb^{2+} detection, the mean = 0.051 V, S_D = 0.009, k_1 = 3, and the smallest detectable volt (E^{ocv}) was calculated as: E^{ocv}_{LOD} = mean + kS_D = 0.078 V. According to the linear regression equation: E^{ocv} = 0.078 log C_{Pb}^{2+} + 1.21, the LOD_3 was calculated to be 3.1 fM. For Hg^{2+} detection, the mean = 0.034 V, S_D = 0.007, k_1 = 3, and the smallest detectable volt (E^{ocv}) was calculated as: E^{ocv}_{LOD} = mean + kS_D = 0.055. According to the linear regression equation: E^{ocv} = 0.083 × log C_{Hg}^{2+} + 1.34, the LOD_4 was calculated to be 3.3 aM.

Movie S1: The smartphone reads out the instantaneous current operation of the self-powered sensor with a capacitor.

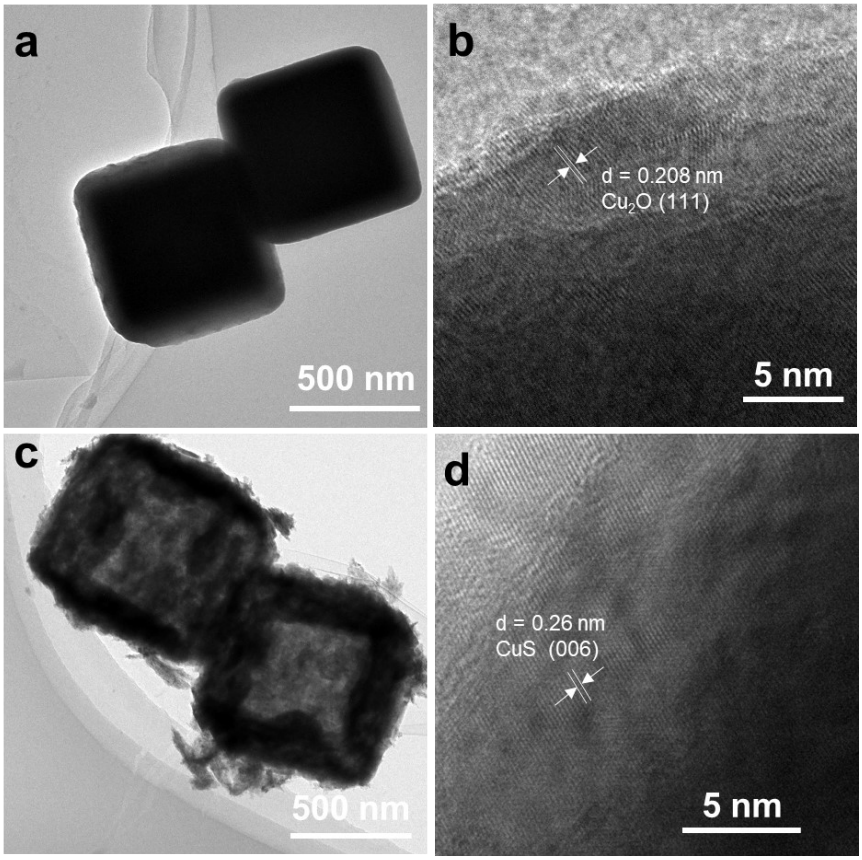

Figure S1. TEM images of Cu_2O templates and CuS nanocubes.

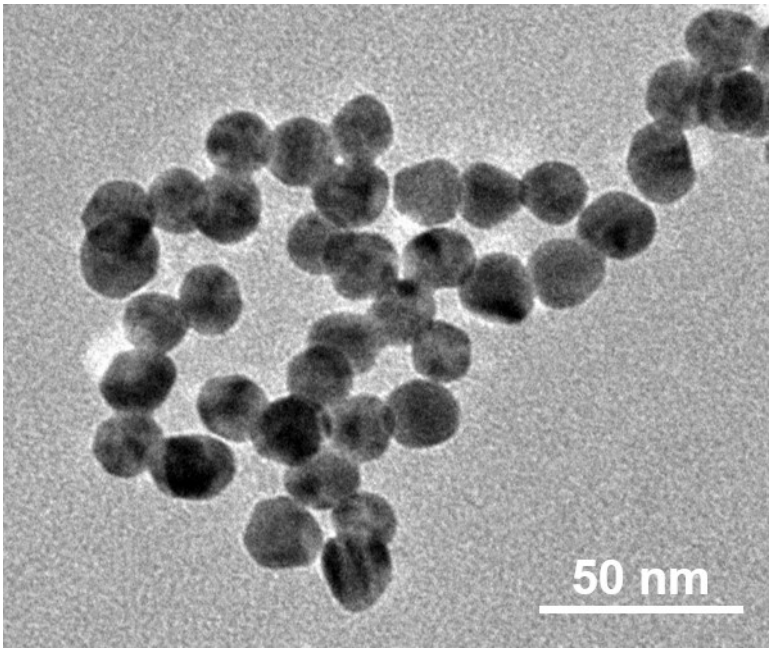

Figure S2. TEM images of AuNPs.

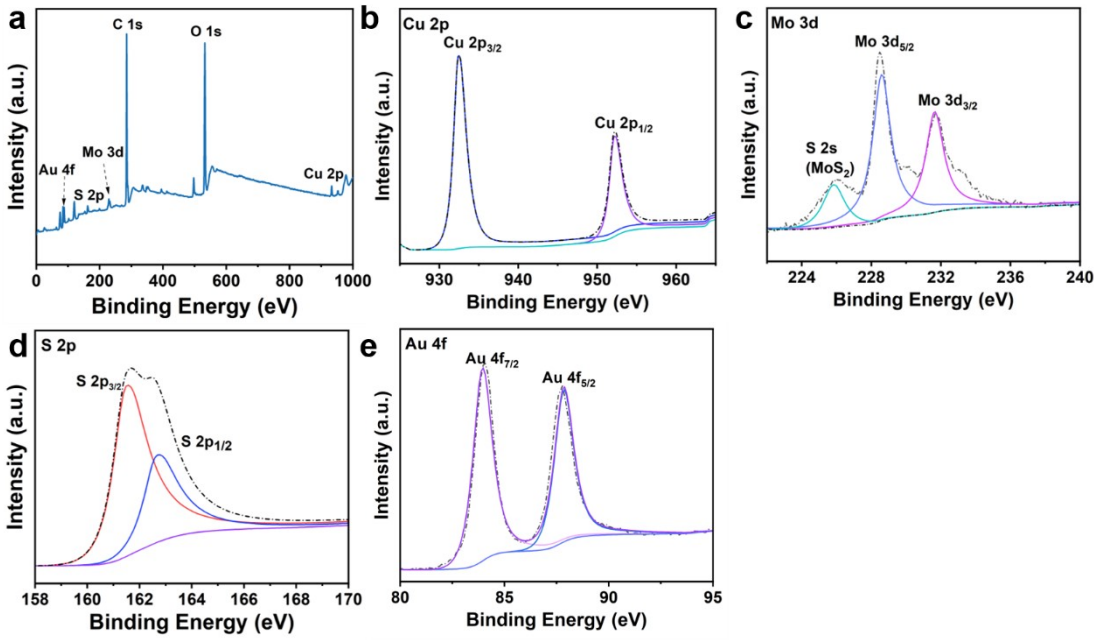

Figure S3. XPS of AuNPs/MoS_2@CuS heterostructures: (a) full spectrum and (b-e) high resolution spectra of Cu 2p, Mo 3d, S 2p, and Au 4f.

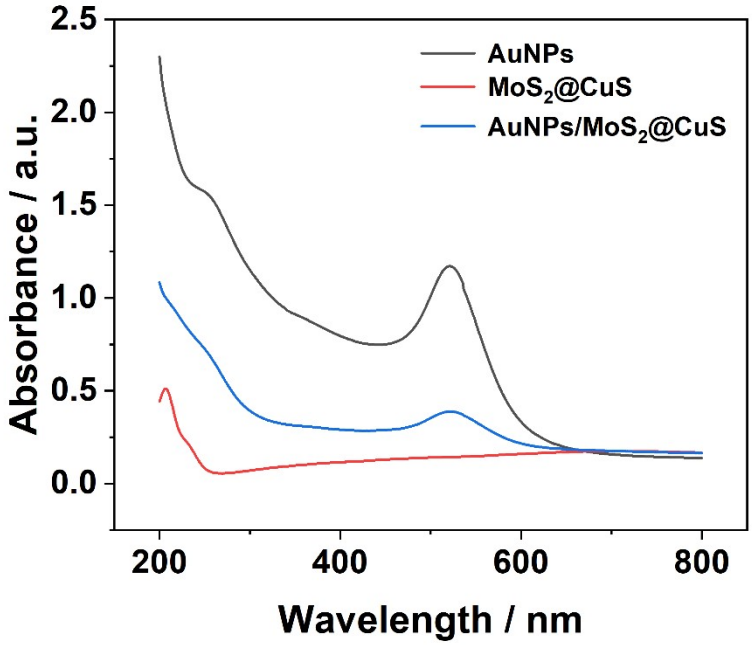

Figure S4. AuNPs, MoS_2@CuS, and AuNPs/MoS_2@CuS heterostructures UV–vis absorption spectra.

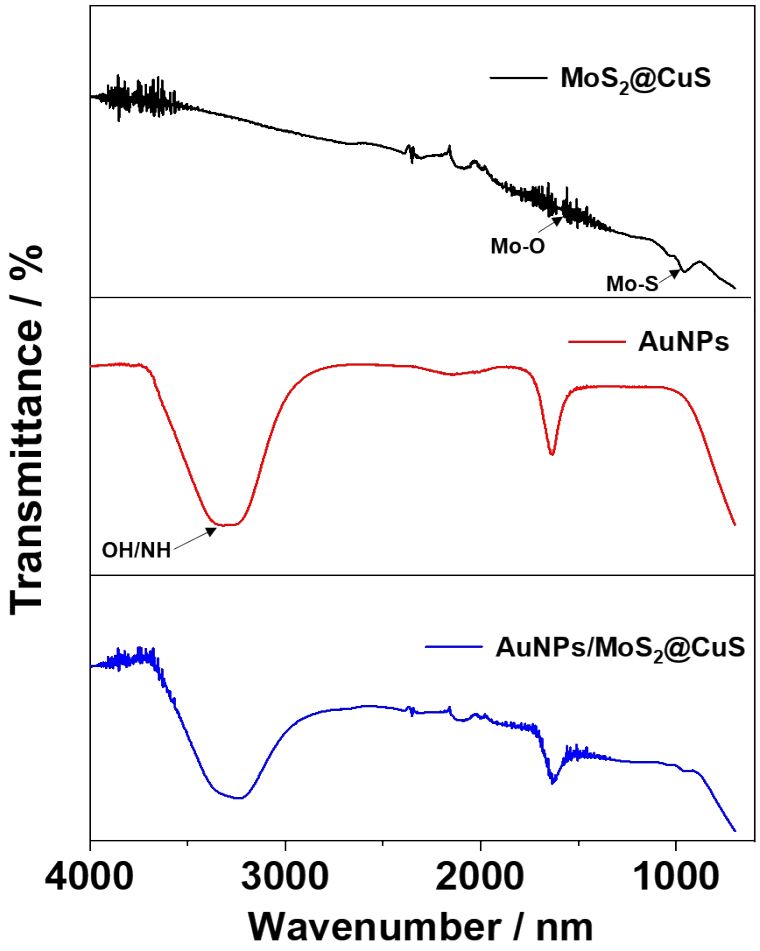

Figure S5. The FITR spectra of AuNPs, MoS_2@CuS, and AuNPs/MoS_2@CuS heterostructures.

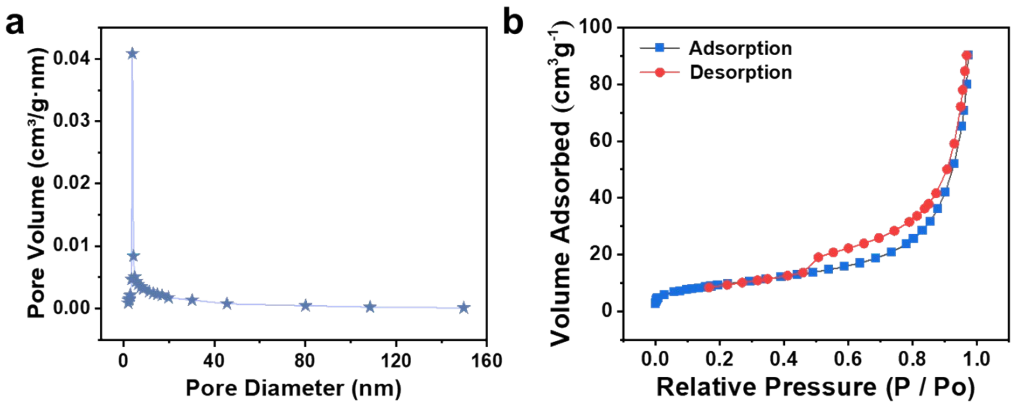

Figure S6. (a) Nitrogen adsorption-desorption isotherms and (b) BET pore size distribution curves of MoS_2@CuS heterostructures.

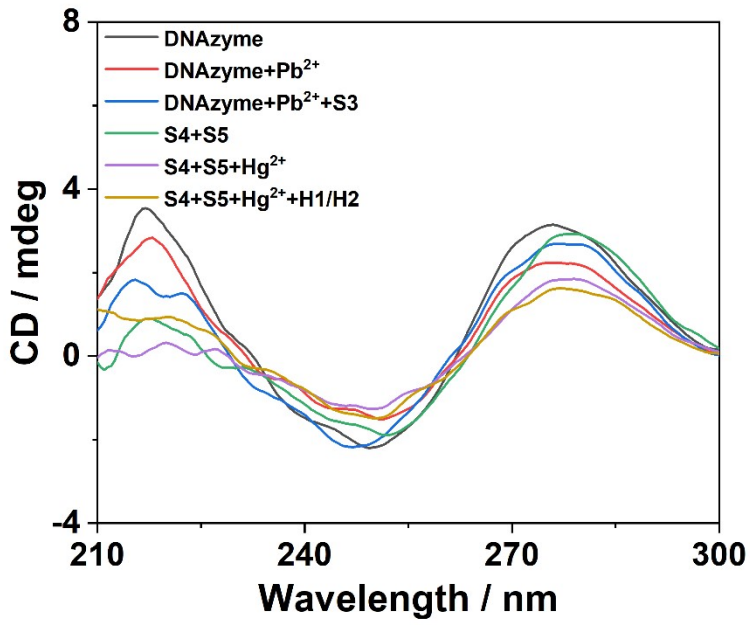

Figure S7. CD spectra for the confirmation of the cutting effect of Pb^{2+} for DNAzyme and T-Hg^{2+}-T complex formation.

Note: For bioanode, the DNAzyme was connected with AuNPs/MoS_2@CuS by Au-S bond, and there was a positive peak at 279 nm and a negative peak at 249 nm, indicating that the DNA has an B-DNA form structure. After Pb^{2+} (10 fM) cut, the amplitude of positive and negative peaks of DNAzyme decreased, but the position of peaks did not change. The cut part, as-split S2 hybridizes with S3 by complementary base pairing, resulting in two weak positive peaks at 215 and 222 nm. For biocathode, the S4 was connected with AuNPs/MoS_2@CuS by Au-S bond, and there was a positive peak at 279 nm and a negative peak at 249 nm corresponding to the B-DNA form structure. Next, Hg^{2+} (10 fM) was added to form a T-Hg^{2+}-T structure, resulting in the disappearance of the positive peak at 215 nm, and the subsequent S4+S5+Hg^{2+}+H1/H2 also disappeared the positive peak at 215 nm, and the negative peak intensity at 249nm increased slightly.

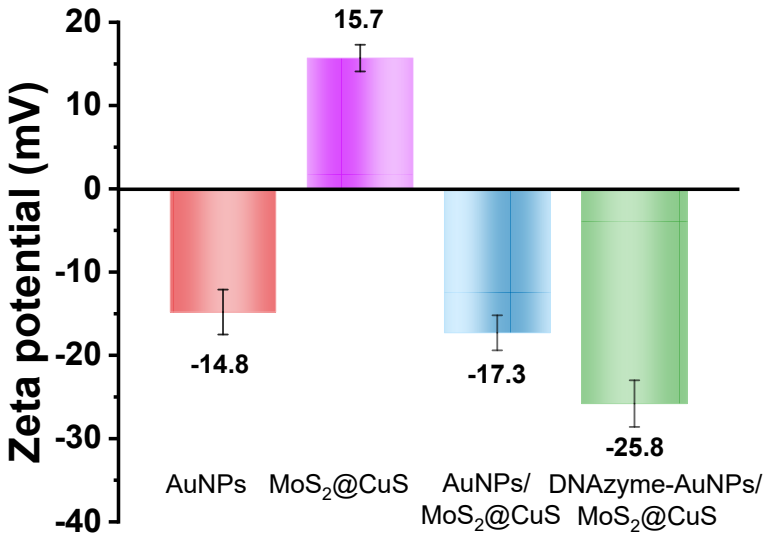

Figure S8. The ζ- potential of AuNPs, MoS_2@CuS heterostructures, AuNPs/MoS_2@CuS and DNAzyme-AuNPs/MoS_2@CuS.

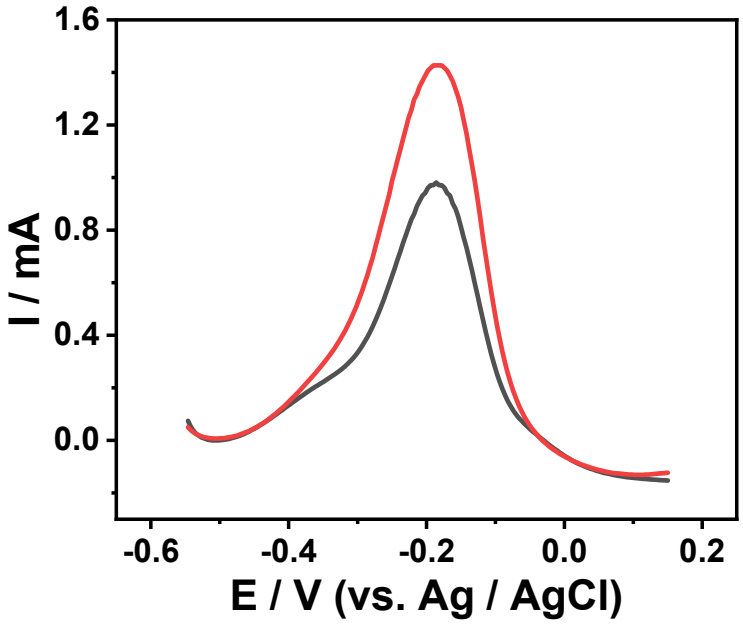

Figure S9. The DPV of detecting 1 nM Hg^{2+} before and after combining the HCR strategy.

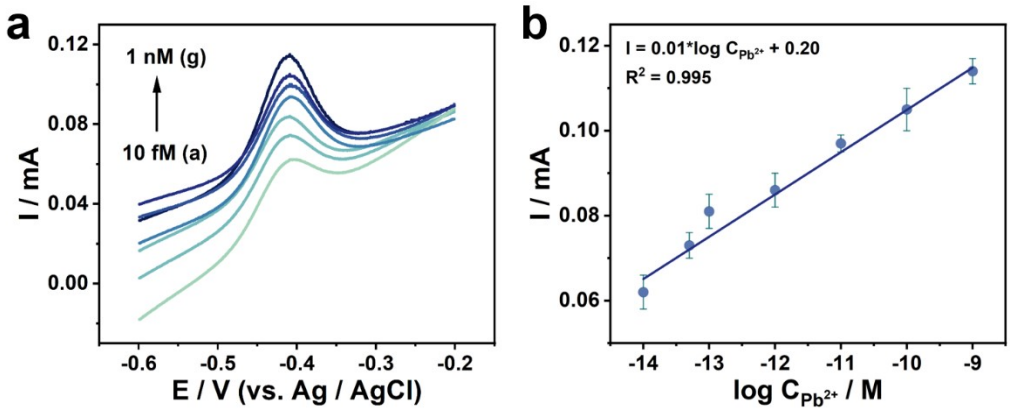

Figure S10. (a) CV curves and (b) linear relationship of the bioanodes with different concentrations of Pb^{2+}.

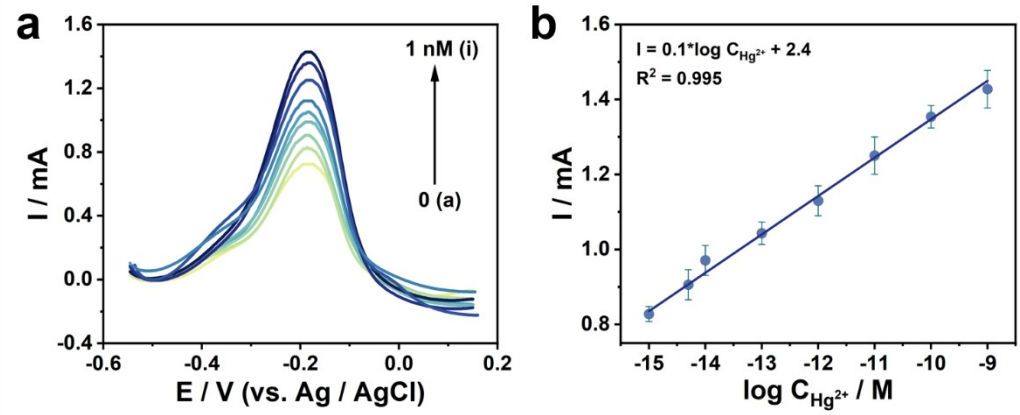

Figure S11. (a) DPV curves and (b) linear relationships of the biocathodes with different concentrations of Hg^{2+}.

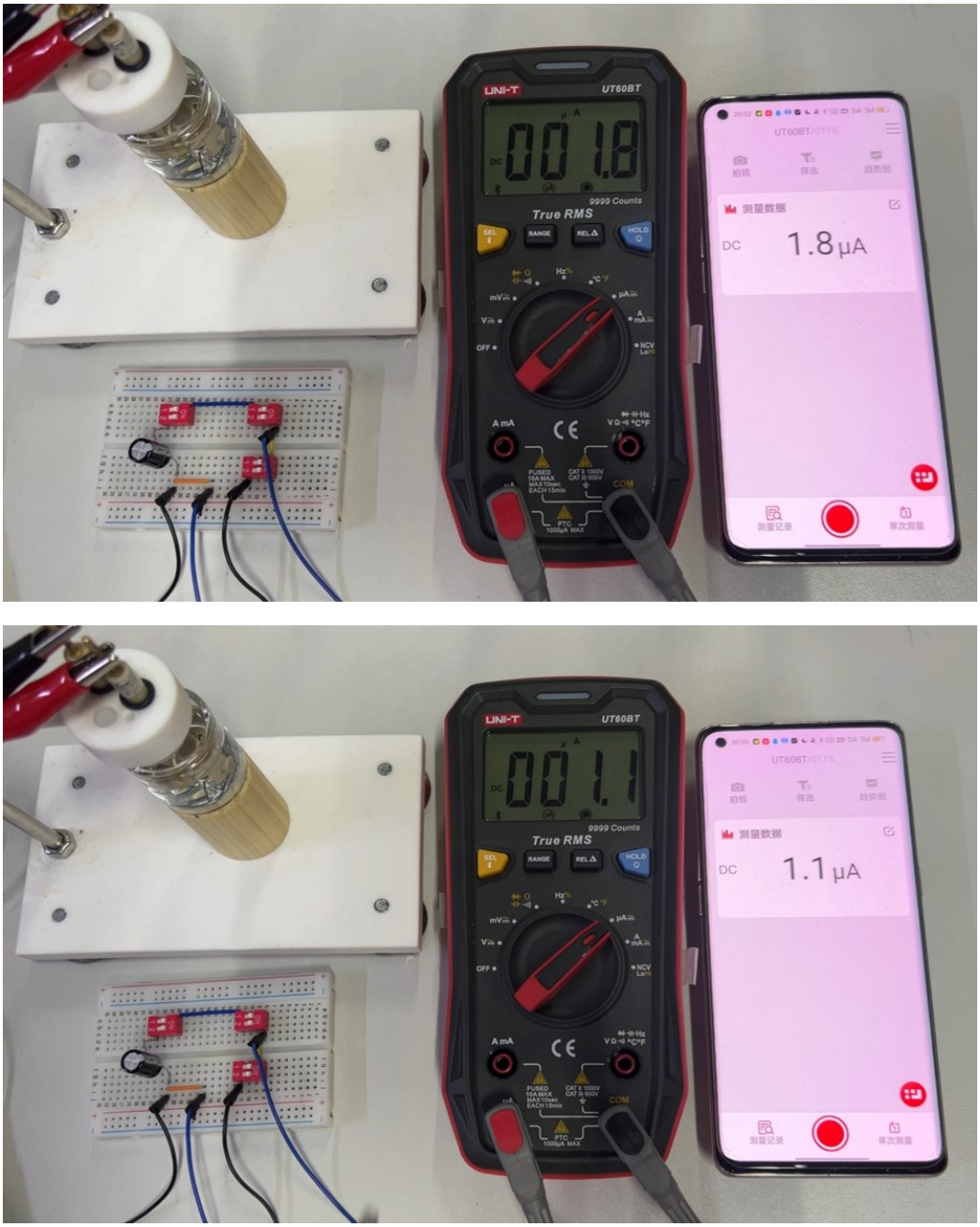

Figure S12. Digital photographs of the smartphone reading out the instantaneous current from the bidirectional self-powered biosensor with a capacitor.

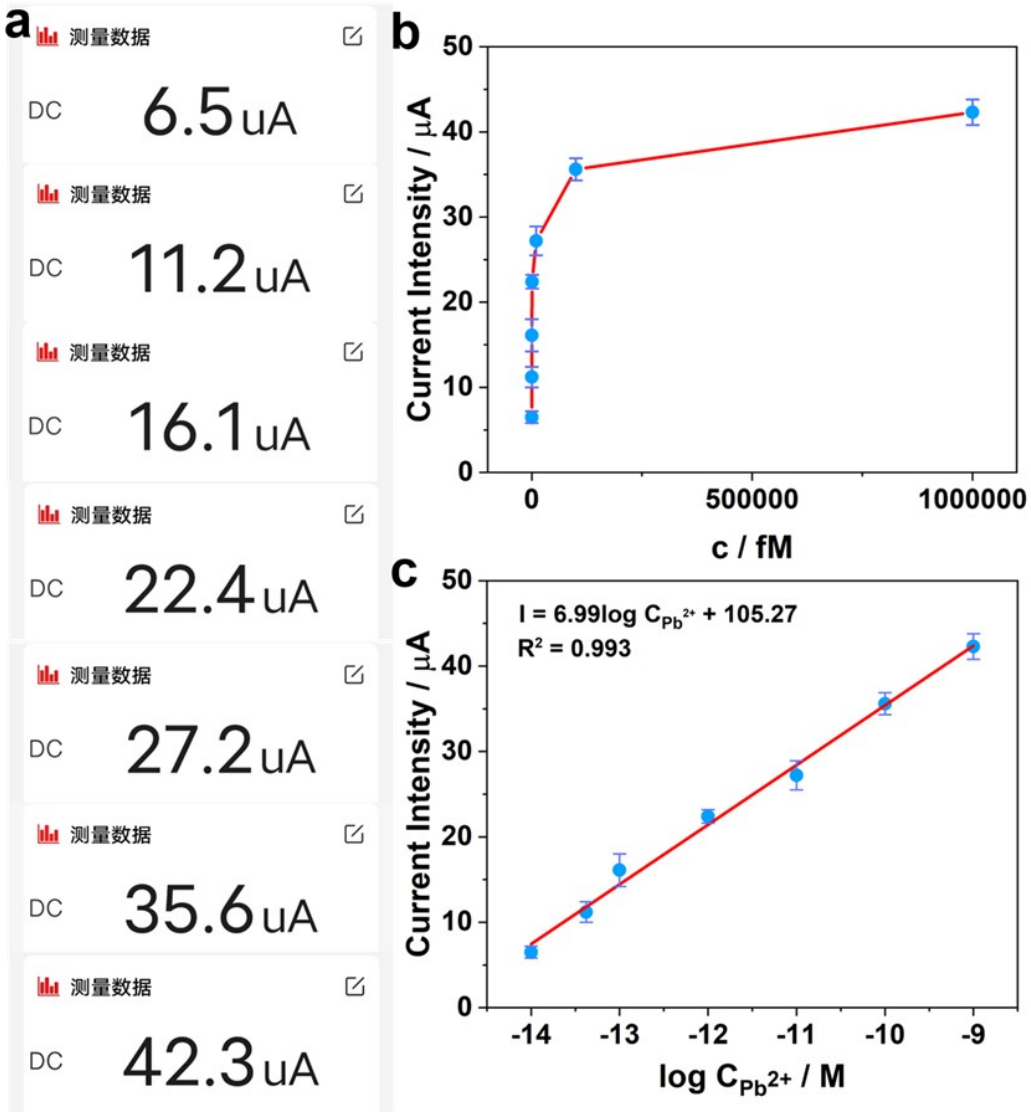

Figure S13. (a) Instantaneous current data received by the smartphonefor different concentrations of Pb^{2+} (b-c) The relationship between the instantaneous current and the concentration of Pb^{2+} displayed by the smartphone.

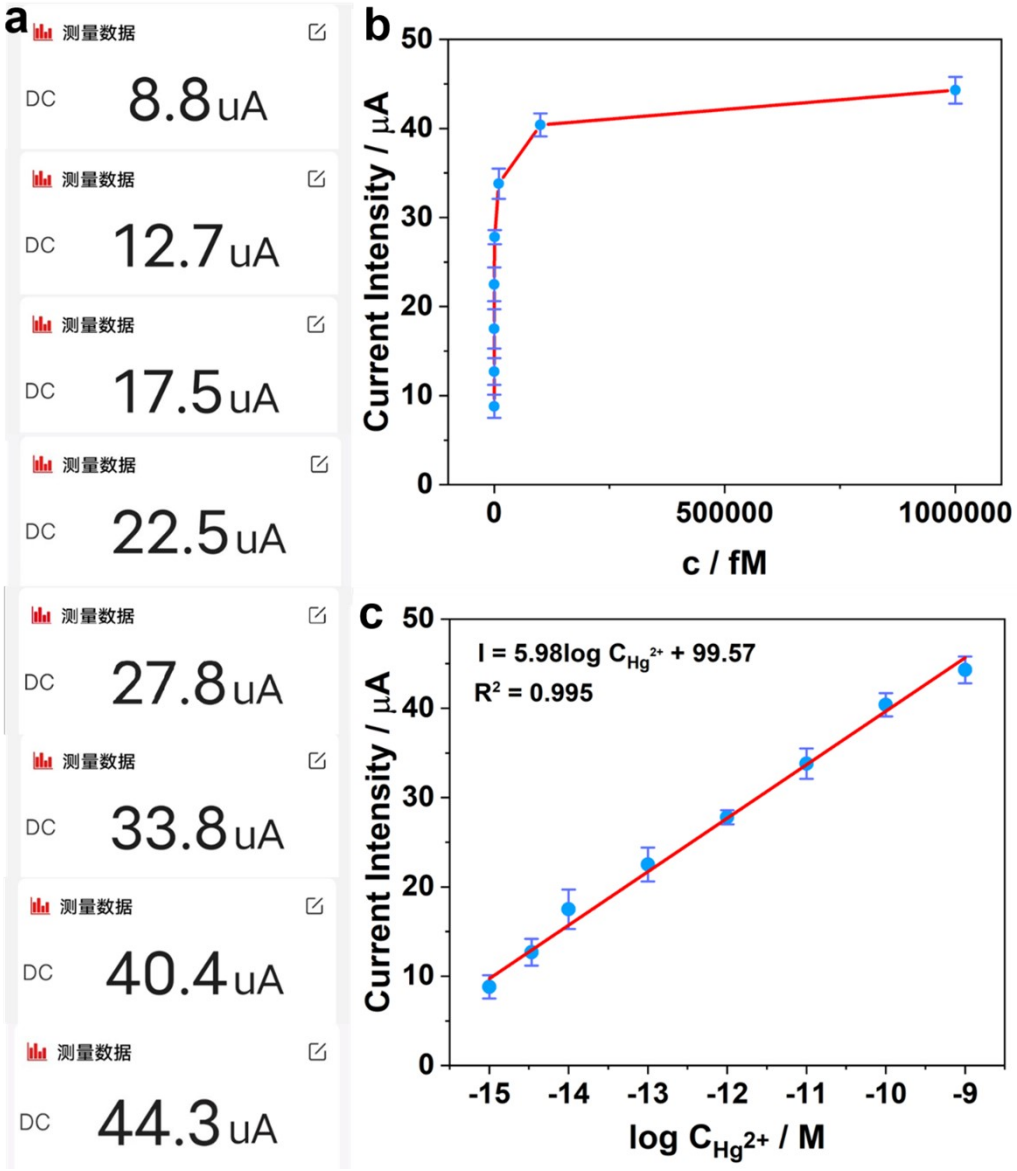

Figure S14. (a) Instantaneous current data received by the smartphone. (b-c) Relationship between the instantaneous current and the concentration of Hg^{2+} displayed by the smartphone.

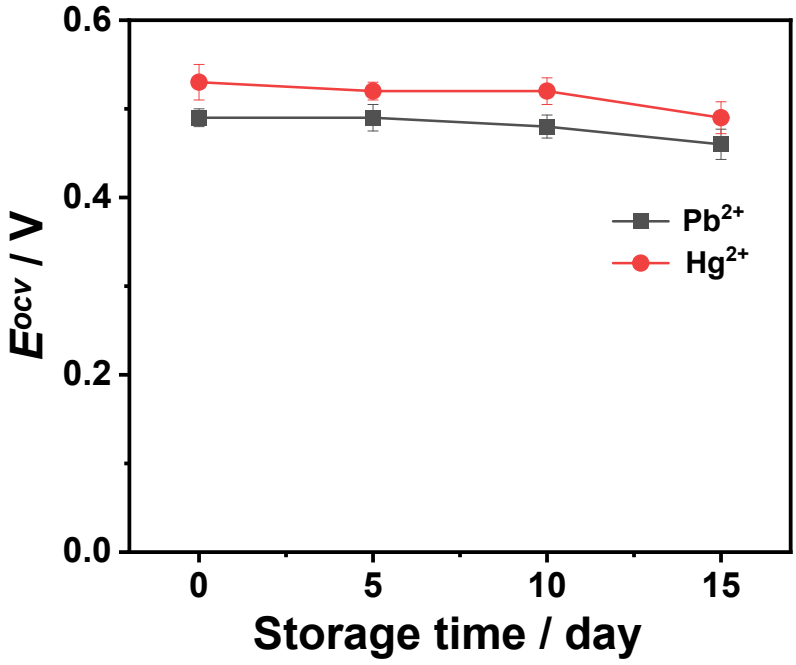

Figure S15. Stability of the bidirectional self-powered biosensor with the 1 nM Pb^{2+} and Hg^{2+}.

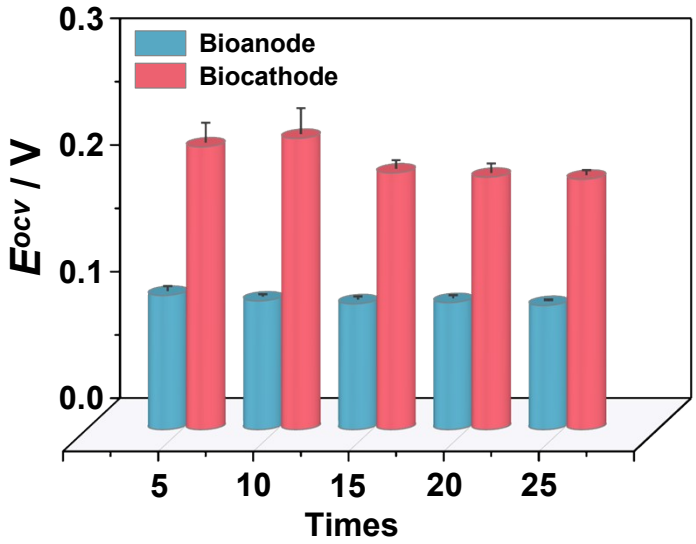

Figure S16. Recyclability of the bidirectional self-powered biosensor.

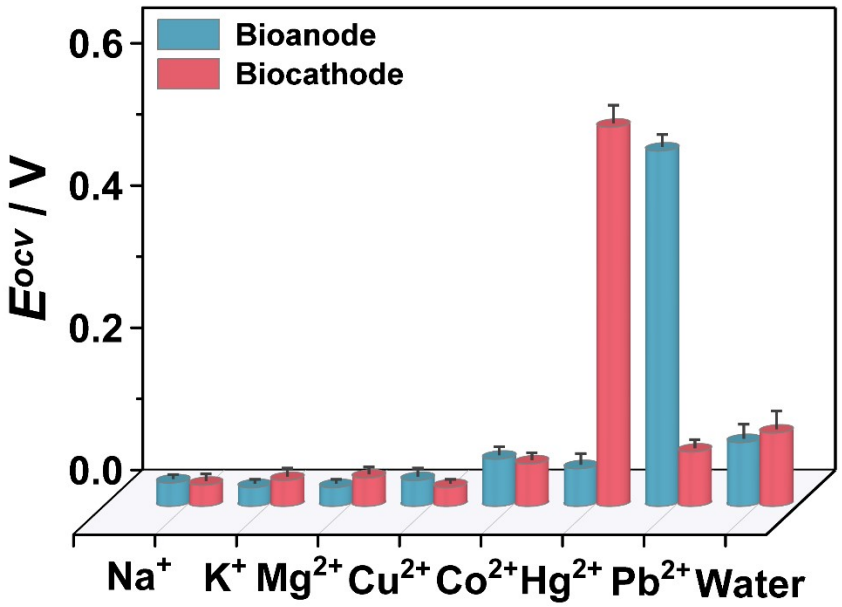

Figure S17. Selectivity of the bioanode and the biocathode.

Table S1. Different sequences of oligonucleotides

Oligonucleotides	Sequences
S1	**5'-**ACTCACTATrAGGAAGAGATG **-3'**
S2	**5'-** HS-$(CH_2)_6$-TTTCATCTCTTCTCCGAGCCGGTCGAAATAGTGAGT **-3'**
S3	**5'-** HS-ACTCACTATTTCGACCGGCTCGGAGAAGAGATG **-3'**
S4	**5'-** HS-$(CH_2)_6$-TTTGCTCTCTCGTTT **-3'**
S5	**5'-**ACTCAATAGCTTTCGTGTGTGCTTT **-3'**
H1	**5'-**GCTATTGAGTCACAATACAG **-3'**
H2	**5'-**ACTCAATAGCCTGTATTGTG **-3'**

Table S2. Comparison of the bidirectional self-powered biosensor with other reported methods for Pb^{2+} detection

Method	Linear range	LOD	References
AC voltammetry (ACV)	0.2 pM - 100 nM	0.048 pM	Cai et al., 2018[1]
Differential pulse voltammetry (DPV)	0.4 pM - 3×10^3 nM	0.27 pM	Huang et al., 2018[2]
Amperometry	5 pM - 1×10^3 nM	2 pM	Yu et al., 2018[3]
Fluorescence	1×10^4 pM - 700 nM	2.7×10^3 pM	Paydar et al., 2022[4]
Electrochemiluminescence	10 pM - 50 nM	4 pM	Zhu et al., 2021[5]
Bidirectional self-powered biosensor	**0.01 pM - 1 nM**	**3.2×10^{-3} pM**	**This work**

Table S3. Comparison of the bidirectional self-powered biosensor with other reported methods for Hg^{2+} detection

Method	Linear range	LOD	References
Electrochemiluminescence	10 fM - 1 nM	0.45 fM	Hang et al., 2018[6]
Differential pulse voltammetry (DPV)	4.9×10^{11} fM - 445×10^{9} fM	13.5×10^{6} fM	Veerakumar et al., 2022[7]
Photoelectrochemical	1×10^{3} fM - 1×10^{4} fM	2×10^{2} fM	Ren et al., 2023[8]
Electrochemiluminescence	1×10^{5} fM - 2×10^{4} fM	5×10^{4} fM	Zhang et al., 2017[9]
Fluorescence	5×10^{7} fM – 5.8×10^{9} fM	3.33×10^{4} fM	Wang et al., 2021[10]
Bidirectional self-powered biosensor	**1 fM - 1×10^{6} fM**	**0.31 fM**	**This work**

Table S4. Analytical results of Pb^{2+} in samples of local sources of tap water (1-4) and lake water (5-8) (n=3)

Water Samples	Added (nM)	Found (nM)	Recovery (%)	RSD (%)
1	1	1.05	105.0	3.9
2	10	10.31	103.1	4.7
3	50	48.23	96.4	5.1
4	100	99.67	99.67	5.3
5	1	0.98	98.0	3.7
6	10	10.39	103.9	5.2
7	50	50.67	101.3	4.8
8	100	102.3	102.3	3.9

Table S5. Analytical results of Hg^{2+} in samples of local sources of tap water (1-4) and lake water (5-8) (n=3)

Water Samples	Added (nM)	Found (nM)	Recovery (%)	RSD (%)
1	1	0.97	97.0	2.1
2	10	10.48	104.8	3.9
3	50	50.4	100.8	4.3
4	100	102.3	102.3	5.9
5	1	1.08	108.0	3.8
6	10	9.93	99.3	4.1
7	50	48.87	97.7	5.8
8	100	103.8	103.8	4.7

Reference

1. Cai, W.; Xie, S.; Zhang, J.; Tang, D.; Tang, Y., Immobilized-free miniaturized electrochemical sensing system for Pb^{2+} detection based on dual Pb^{2+}-DNAzyme assistant feedback amplification strategy. *Biosens. Bioelectron.* **2018,** *117*, 312-318.
2. Huang, X.; Li, J.; Zhang, Q.; Chen, S.; Xu, W.; Wu, J.; Niu, W.; Xue, J.; Li, C., A protease-free and signal-on electrochemical biosensor for ultrasensitive detection of lead ion based on GR-5 DNAzyme and catalytic hairpin assembly. *J. Electroanal. Chem.* **2018,** *816*, 75-82.
3. Yu, Y.; Yu, C.; Niu, Y.; Chen, J.; Zhao, Y.; Zhang, Y.; Gao, R.; He, J., Target triggered cleavage effect of DNAzyme: Relying on Pd-Pt alloys functionalized Fe-MOFs for amplified detection of Pb^{2+}. *Biosens. Bioelectron.* **2018,** *101*, 297-303.
4. Paydar, S.; Feizi, F.; Shamsipur, M.; Barati, A.; Chehri, N.; Taherpour, A.; Jamshidi, M., An ideal ratiometric fluorescent probe provided by the surface modification of carbon dots for the determination of Pb^{2+}. *Sens. Actuators, B* **2022,** *369*, 132243.
5. Zhu, L.; Lv, X.; Li, Z.; Shi, H.; Zhang, Y.; Zhang, L.; Yu, J., All-sealed paper-based electrochemiluminescence platform for on-site determination of lead ions. *Biosens. Bioelectron.* **2021,** *192*, 113524.
6. Hang, X.-M.; Zhao, K.-R.; Wang, H.-Y.; Liu, P.-F.; Wang, L., Exonuclease III-assisted CRISPR/Cas12a electrochemiluminescence biosensor for sub-femtomolar mercury ions determination. *Sens. Actuators, B* **2022,** *368*, 132208.
7. Veerakumar, P.; Jaysiva, G.; Chen, S.-M.; Lin, K.-C., Development of Palladium on Bismuth Sulfide Nanorods as a Bifunctional Nanomaterial for Efficient Electrochemical Detection and Photoreduction of Hg(II) Ions. *ACS Appl. Mater. Interfaces* **2022,** *14* (4), 5908-5920.
8. Ren, X.; Chen, J.; Wang, C.; Wu, D.; Ma, H.; Wei, Q.; Ju, H., Photoelectrochemical Sensor with a Z-Scheme Fe(2)O(3)/CdS Heterostructure for Sensitive Detection of Mercury Ions. *Anal. Chem.* **2023,** *95* (46), 16943-16949.
9. Zhang, Y.; Zhang, C.; Ma, R.; Du, X.; Dong, W.; Chen, Y.; Chen, Q., An ultra-sensitive Au nanoparticles functionalized DNA biosensor for electrochemical sensing of mercury ions. *Mater. Sci. Eng. C* **2017,** *75*, 175-181.
10. Wang, S.; Chen, H.; Xie, H.; Wei, L.; Xu, L.; Zhang, L.; Lan, W.; Zhou, C.; She, Y.; Fu, H., A novel thioctic acid-carbon dots fluorescence sensor for the detection of Hg^{2+} and thiophanate methyl via S-Hg affinity. *Food Chemistry* **2021,** *346*, 128923.